

Wave reflections in the pulmonary arteries analysed with the reservoir–wave model

J. Christopher Bouwmeester¹, Israel Belenkie^{1,2,3}, Nigel G. Shrive⁴ and John V. Tyberg^{1,2,5}

¹Libin Cardiovascular Institute of Alberta, ²Departments of Cardiac Sciences, ³Medicine, ⁴Civil Engineering and ⁵Physiology and Pharmacology, University of Calgary, Calgary, Alberta, Canada

Key points

- In the pulmonary artery, we use the reservoir–wave model to separate the effects of a charging and discharging, elastic arterial reservoir from the effects of waves created by the contracting and relaxing heart.
- Wave intensity analysis quantifies the effects of waves that cause changes in pressure and flow and precisely identifies when waves created by the heart and reflections of these waves start and end.
- We show that negative wave reflections arise from the junction of lobar arteries stemming from the left and right pulmonary arteries.
- When blood volume is increased and pulmonary arteries become distended, the strength of negative wave reflections increases when 100% O₂ is used for ventilation.
- Negative reflections suck blood downstream and, as they arrive when the heart is developing maximal pressure, negative reflections help to lower the back pressure the heart must pump against and, thus, they tend to increase the forward flow of blood.

Abstract Conventional haemodynamic analysis of pressure and flow in the pulmonary circulation yields incident and reflected waves throughout the cardiac cycle, even during diastole. The reservoir–wave model provides an alternative haemodynamic analysis consistent with minimal wave activity during diastole. Pressure and flow in the main pulmonary artery were measured in anaesthetized dogs and the effects of hypoxia and nitric oxide, volume loading and positive end-expiratory pressure were observed. The reservoir–wave model was used to determine the reservoir contribution to pressure and flow and once subtracted, resulted in ‘excess’ quantities, which were treated as wave-related. Wave intensity analysis quantified the contributions of waves originating upstream (forward-going waves) and downstream (backward-going waves). In the pulmonary artery, negative reflections of incident waves created by the right ventricle were observed. Overall, the distance from the pulmonary artery valve to this reflection site was calculated to be 5.7 ± 0.2 cm. During 100% O₂ ventilation, the strength of these reflections increased 10% with volume loading and decreased 4% with 10 cmH₂O positive end-expiratory pressure. In the pulmonary arterial circulation, negative reflections arise from the junction of

lobar arteries from the left and right pulmonary arteries. This mechanism serves to reduce peak systolic pressure, while increasing blood flow.

(Received 17 February 2014; accepted after revision 16 April 2014; first published online 22 April 2014)

Corresponding author J. C. Bouwmeester: Yale University School of Medicine, Department of Surgery, Brady Memorial Laboratory, Room 211, 310 Cedar Street, New Haven, CT 06510, USA. Email: james.bouwmeester@yale.edu

Abbreviations BCW, backward compression wave; BDW, backward decompression wave; C, reservoir compliance; c , wave speed; FCW, forward compression wave; FDW, forward decompression wave; P_{∞} , asymptotic pressure; PA, pulmonary artery; P_{backward} , backward-going wave pressure; PEEP, positive end-expiratory pressure; P_{excess} , excess pressure; P_{forward} , forward-going wave pressure; P_{PA} , pulmonary artery pressure; P_{res} , reservoir pressure; PV, pulmonary vein; Q_{excess} , excess flow; Q_{in} , pulmonary arterial reservoir inflow; Q_{out} , pulmonary arterial reservoir outflow; Q_{PA} , pulmonary artery flow; Q_{res} , pulmonary arterial reservoir flow; R , reservoir resistance; RV, right ventricle/ventricular; U_{backward} , backward-going wave velocity; U_{excess} , excess velocity; U_{forward} , forward-going wave velocity; U_{PA} , pulmonary artery velocity; WIA, wave intensity analysis; WI_{backward} , backward-going wave intensity; WI_{excess} , excess wave intensity; WI_{forward} , forward-going wave intensity; Γ , reflection ratio; δt , delay of reflected wave.

Introduction

Conventional haemodynamic approaches attribute the measured pressure and flow to be the result of waves created by the cardiac chambers and reflections of these incident waves (Westerhof 1972; Hughes & Parker, 2009). In vascular systems, reflections can occur from branch points and therefore first appear downstream from the heart and travel backwards (i.e. against the direction of net blood flow). However, recent re-evaluation of these conventions suggests a pattern that defies physiological expectations: wave reflections appear first at the aortic valve and travel forwards (i.e. in the direction of net blood flow) (Wang *et al.* 2011; Tyberg *et al.* 2013; Westerhof & Westerhof, 2013). Therefore, a paradox occurs when, by definition, forward-going waves are created by the heart and backward-going waves are created by reflections.

The reservoir–wave model has been used to describe intuitive patterns of aortic wave propagation and reflection in the aorta, where downstream branch points cause incident waves to be reflected back to the aortic valve (Wang *et al.* 2003, 2011, 2013). This model provides an alternative understanding of pulmonary haemodynamics (Bouwmeester *et al.* 2013) and other vascular systems (Wang *et al.* 2003, 2006, 2008, 2011, 2013; Flewitt *et al.* 2007; Tyberg *et al.* 2009; Davies *et al.* 2010) by considering the contribution of a reservoir to measured pressure and flow. When applied to the pulmonary arterial circulation, the reservoir is based on a two-element windkessel (Frank, 1899; Sagawa *et al.* 1990), modified to take into account the zero flow (critical closing) pressure of alveolar blood vessels (Permutt & Riley, 1963). Once the reservoir pressure or flow is defined it is subtracted and the resulting wave-related ‘excess’ components of pressure and flow are analysed using wave intensity analysis (WIA) (Parker & Jones, 1990). WIA describes waves as they occur in time and quantifies the effects of waves on pressure and velocity/flow, where the prototypical wave is the forward

compression wave (FCW) generated by the ventricle at the start of ejection.

The goal for a haemodynamic model of the pulmonary circulation should include the ability to discriminate between the various causes of pulmonary hypertension, either through an assessment of vascular properties or the analysis of propagated and reflected waves. Pioneering studies used Fourier analysis to determine the hydraulic impedance of the pulmonary circulation (Caro & McDonald, 1961; Patel *et al.* 1963) and further study of pulmonary hypertension showed that both arterial compliance and resistance have important contributions to right ventricular afterload (Milnor *et al.* 1969). To understand these contributions, Westerhof’s three-element windkessel model (Westerhof *et al.* 1971) provides a good platform to quantify the independent contributions of lumped pulmonary vascular resistance and compliance (Elzinga *et al.* 1980). Determining these lumped vascular properties can be used to distinguish the differences between idiopathic and chronic thromboembolic pulmonary hypertension (Lankhaar *et al.* 2006, 2008; Saouti *et al.* 2010), which have distinct pressure waveforms and potentially different patterns of wave propagation and reflection (Nakayama *et al.* 1997; Castelain *et al.* 2001).

The reservoir–wave model provides a method to measure the separate contributions of lumped vascular properties with reservoir behaviour and the effects of wave propagation and reflection. Therefore, it is possible that this approach would help clarify the pathophysiology of various types of pulmonary hypertension. In the present study, we used the reservoir–wave model to describe the response of the normal pulmonary arterial circulation to decreased vascular resistance (with volume loading), potential collapse of small pulmonary vessels [with positive end-expiratory pressure (PEEP)], and active vasoconstriction and vasodilation (with hypoxia and inhaled nitric oxide, respectively).

Methods

Animal preparation

The University of Calgary animal care committee, whose criteria conformed to the 'Guiding Principles for Research Involving Animals and Human Beings' of the American Physiological Society, granted ethical approval of all experimental protocols. Anaesthesia was induced in 11 mongrel dogs (seven male; 18–28 kg, mean 22 kg) with an initial i.v. injection of 25 mg kg⁻¹ sodium thiopental and anaesthesia was maintained with an infusion of fentanyl (20–30 μg kg⁻¹ h⁻¹) and midazolam (0.01–0.015 μg kg⁻¹ h⁻¹). The dogs were ventilated using a constant volume respirator (model 607; Harvard Apparatus Inc., Natick, MA, USA) with a 50% O₂, 50% nitrous oxide gas mixture during surgery and with 100% O₂ during experimentation. The respiratory rate (16–18 breaths min⁻¹) and tidal volume (15 ml kg⁻¹) were adjusted to maintain physiological arterial blood gas levels ($P_{a,CO_2} = 35\text{--}45$ mmHg) and pH (7.2–7.4) (Mitchell *et al.* 2011). Body temperature was kept at 37°C by using a circulating warm-water blanket and heat lamp when necessary. A bladder catheter was inserted into the urethra to collect urine. During experimentation, the dogs were ventilated with 100% O₂ using a different ventilator (Servo Ventilator 900C; Siemens-Elima AB, Solna, Sweden) that allowed quick adjustment of minute ventilation, respiratory rate and PEEP. The chest remained open to allow access to the measuring devices that sometimes required adjustment.

The experimental instrumentation has been described previously (Bouwmeester *et al.* 2013). Briefly, pressure was measured in the right ventricle (RV), left ventricle and left atrium with 7-F catheter-tip pressure transducers with lumens (Scisense Inc., London, Ontario, Canada) and in the main pulmonary artery (PA) and a single pulmonary vein (PV) with 3.5-F catheter-tip pressure transducers without lumens (Millar Instruments Inc., Houston, TX, USA). The PA catheter was inserted through the anterior wall of the RV and advanced approximately 1 cm beyond the pulmonary valve. The PV catheter was placed in a left-sided PV, approximately 1 cm upstream of the left atrium. Flow probes (A- and S-Series models and flowmeter model T206; Transonic Systems, Ithaca, NY, USA) were placed on the main PA (immediately downstream of the tip of the PA catheter) and the PV (immediately upstream of the tip of the PV catheter). A four-lead ECG was also recorded. After instrumentation was complete, the pericardium was reapproximated with interrupted loose sutures (Scott-Douglas *et al.* 1991).

Electronic signals were sampled at 400 Hz with data acquisition software (Sonometric Corp., London, Ontario, Canada) and data were analysed using CV Works (AccuDAQ Inc., Calgary, Alberta, Canada).

Experimental protocol

Volume loading was assessed by mean pulmonary venous pressure, which was sequentially increased with an infusion of 10% pentastarch solution (Pentastan; Bristol-Myers Squibb Canada, Montreal, Quebec, Canada) to achieve low (~5 mmHg), medium (~9 mmHg) and high (~14 mmHg) filling pressures. At each filling pressure, three ventilation strategies were used: (1) 100% O₂; (2) hypoxia; and (3) hypoxia plus nitric oxide. Ventilation with 100% O₂ was used as a baseline; hypoxia was induced by adding N₂ to the inspired gas mixture until P_{a,O_2} was less than 50 mmHg. Then, during hypoxic ventilation, nitric oxide was added (80 ppm) to the inspired gas mixture (INOvent delivery system; Datex-Ohmeda, Helsinki, Finland). At each ventilation state, recordings were taken at 0 and 10 cmH₂O PEEP, the order of which was randomly selected.

At the conclusion of the experiments, while deeply anaesthetized, the dogs were killed with an intracardiac injection of KCl.

Reservoir analysis

The pulmonary arterial reservoir model used by Bouwmeester *et al.* (2013) was based upon earlier work (Wang *et al.* 2003) and was used to describe the PA reservoir pressure (P_{res}) as follows:

$$\frac{dP_{res}(t)}{dt} = \frac{Q_{in}(t) - Q_{out}(t)}{C}$$

$$\text{Where: } Q_{out}(t) = \frac{P_{res}(t) - P_{\infty}}{R} \quad (1)$$

$$P_{res}(t) = P_{\infty} + (P_0 - P_{\infty})e^{-\frac{t}{RC}} + e^{-\frac{t}{RC}} \int_{t_0}^t \frac{Q_{in}(t')}{C} e^{\frac{t'}{RC}} dt' \quad (2)$$

For the arterial reservoir, inflow provided to this reservoir is easily measured and equivalent to measured main PA flow ($Q_{PA} \equiv Q_{in}$), while arterial outflow (Q_{out}) provided to the pulmonary capillaries is much more difficult to measure and therefore, modelled by eqn (1). Equation (2) represents the analytical solution to eqn (1), where P_0 and t_0 represent the time and PA pressure at the onset of ejection and R , C and P_{∞} are the arterial reservoir parameters.

To determine the reservoir pressure in eqn (2), the reservoir parameters were assumed to be constant over the range of pressures measured during each intervention. Initial estimates of reservoir parameters were made and P_{res} was calculated throughout a complete cardiac

cycle. The initial estimates are arbitrary and appropriate values for reservoir parameters were determined using an algorithm developed in Matlab (Mathworks, Natick, MA, USA) employing the function 'fminsearch' (Nelder–Mead simplex algorithm) to vary these parameters iteratively to minimize the mean-squared error between P_{res} and P_{PA} during diastole. This method is robust and relatively insensitive to the initial reservoir parameter estimates. The result of this procedure applied to the PA is shown in Fig. 1, where it was assumed that the exponential decline of P_{PA} during mid-to-late (approximately last two-thirds) diastole represented a decreasing reservoir pressure and therefore was used to calculate P_{res} .

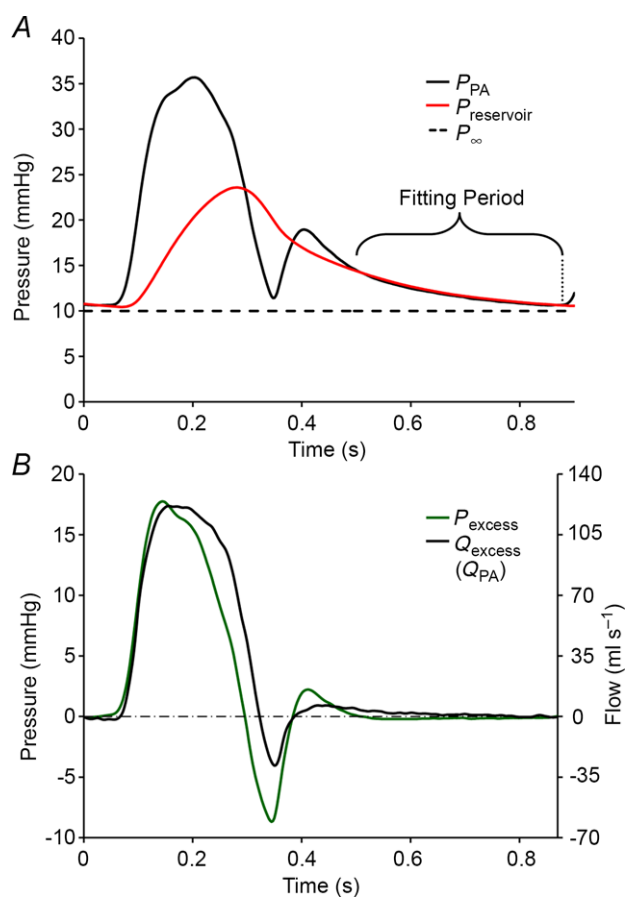


Figure 1. Illustrating how pulmonary artery pressure and flow were analysed and showing pulmonary artery reservoir and excess pressure

Data are taken during low blood volume, 0 cmH₂O positive end-expiratory pressure and 100% O₂ ventilation. A, measured pulmonary artery pressure (P_{PA}), pulmonary artery reservoir pressure (P_{res}) and pulmonary artery asymptotic pressure (P_{∞}). B, excess pulmonary artery pressure (P_{excess}) is shown on the left y-axis and excess pulmonary artery flow (Q_{excess}), which in the main pulmonary artery is equivalent to measured pulmonary artery flow (Q_{PA}), is shown on the right y-axis.

Excess pressure and flow/velocity

Excess pressure or flow is calculated by subtracting the reservoir contribution from the measured pressure or flow. In the PA, excess pressure (P_{excess}) is calculated by subtracting P_{res} from P_{PA} ($P_{\text{excess}} = P_{\text{PA}} - P_{\text{res}}$). In general, excess flow (Q_{excess}) is also calculated by subtracting reservoir flow (Q_{res}) from Q_{PA} ($Q_{\text{excess}} = Q_{\text{PA}} - Q_{\text{res}}$). However, the main PA is a unique location, in that there is no reservoir upstream and measured flow is negligible during diastole when the pulmonary valve is closed. Since the reservoir contribution is determined during diastole and because there is no reservoir upstream of the main PA, Q_{res} in this location is zero. Therefore, in the main PA Q_{excess} is equal to Q_{PA} . (NB if flow were measured further downstream, the reservoir upstream of that location would discharge, resulting in significant Q_{res} that would need to be subtracted to determine Q_{excess} at that location). P_{excess} and Q_{excess} waveforms are shown in Fig. 1B. For the purposes of WIA, Q_{excess} is converted to velocity (U_{excess}) as follows: $U_{\text{excess}} = Q_{\text{excess}}/A$; where the cross-sectional area (A) of the main PA was estimated from the diameter of the flow probe attached to it.

Wave intensity analysis

Defined by WIA, there are four types of waves that have different effects on pressure and velocity and, in the context of this study, account for changes in P_{excess} and U_{excess} . The forward direction is defined as the direction of net blood flow and waves might either increase (compression waves) or decrease (decompression waves) pressure as they pass. Thus, there are FCW or backward compression waves (BCW) and forward (FDW) or backward (BDW) decompression waves. In this study, the RV generates forward waves, which are transmitted downstream and backward waves arriving during systole are reflections of these incident waves. Forward waves can be separated from backward waves if the local wave speed is known (Parker, 2009). In the PA, the single point wave speed was calculated using the linear regression of the $P_{\text{excess}}/U_{\text{excess}}$ relationship during the upstroke of systole (Khiri *et al.* 2001) when only a FCW was assumed to be present.

WIA of P_{excess} and U_{excess} and the calculation of reflector distance and magnitude are shown in Fig. 2A. Excess wave intensity (WI_{excess}) is decomposed into the intensities of forward- and backward-going waves (WI_{forward} and WI_{backward} , respectively). To quantify the pressure effects of these waves, the incremental pressure changes of forward- and backward-going waves were integrated (P_{forward} and P_{backward} respectively) as shown in Fig. 2B, where the onsets of incident waves (FCW and FDW, respectively) and their reflections (BDW and BCW, respectively) are labelled. The intervals between the onsets of incident and reflected waves are indicated by δt . Together with

the single-point wave speed (c), δt is used to estimate the distance from the measurement to the reflection site [$d = c (\delta t/2)$], assuming no change in the wave speed and vascular properties between where it is detected and the reflection site. The magnitude of the reflection is measured by the reflection ratio (Γ), which is calculated as: [$\Gamma = \Delta P_{\text{backward}}/\Delta P_{\text{forward}}$]. Taking into account experimental and analytical errors, reflections were only considered significant if the absolute value of Γ was greater than 0.15, which correlates with the ratio of daughter/mother vessels (in terms of cross-sectional area) of ~ 0.8 – 0.9 for positive reflections and ~ 1.3 – 1.5 for negative reflections (Parker, 2009).

Statistical methods

All data were analysed with SigmaPlot software (Systat Software Inc., San Jose, CA, USA). Three-way ANOVA

was used to analyse the effects of volume load, PEEP and ventilation (see Table 1). Owing to incomplete data sets, the results are presented as least-squared mean values (estimated using a general linear model) \pm S.E.M. For all statistical tests, the significance level was set at 0.05. Pairwise multiple comparisons were made with the Bonferroni method.

Results

The RV creates two incident waves as shown by WIA of P_{excess} and U_{PA} in Fig. 2. The FCW is generated at the beginning of systole with initial contraction and the FDW is generated mid-systole when RV contraction starts to decelerate. Negative reflections are observed as the FCW is reflected as BDW and the FDW is reflected as BCW. The magnitude of the negative Γ is expressed in absolute terms,

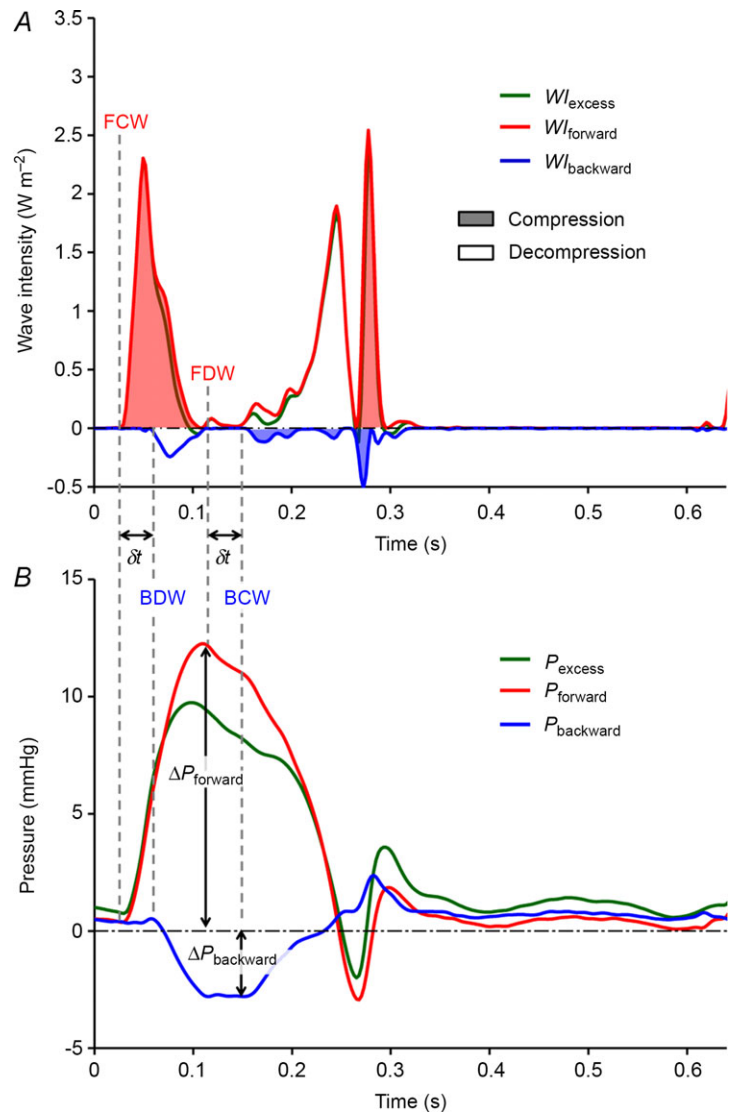


Figure 2. Wave intensity analysis of pulmonary artery excess pressure and velocity

Data are taken during low blood volume, 0 cmH₂O positive end-expiratory pressure and 100% O₂ ventilation. A, net wave intensity (Wl_{excess}) is decomposed into forward-going (Wl_{forward}) and backward-going (Wl_{backward}) wave components. The wave energy of compression waves is represented by shaded areas and decompression waves by open areas. B, P_{excess} is decomposed into the contributions of forward-going (P_{forward}) and backward-going (P_{backward}) waves. Onsets of FCW, FDW, BCW and BDW are indicated by vertical dashed lines. δt indicates the interval between the incident forward-going waves and reflected backward-going waves (i.e. FCW \rightarrow BDW and FDW \rightarrow BCW). The reflection ratio (Γ) is equal to $\Delta P_{\text{backward}}/\Delta P_{\text{forward}}$. BCW, backward compression wave; BDW, backward decompression wave; FCW, forward compression wave; FDW, forward decompression wave.

Table 1. Pulmonary artery reservoir parameters and wave analysis results

	Low volume	Medium volume	High volume	PEEP 0 cmH ₂ O	PEEP 10 cmH ₂ O	100% O ₂	Hypoxia	Nitric oxide
Reservoir parameters								
<i>R</i> (mmHg s ⁻¹ ml ⁻¹)	0.28 ± 0.01*[‡]	0.22 ± 0.02*[†]	0.16 ± 0.02^{†‡}	0.22 ± 0.01	0.22 ± 0.01	0.19 ± 0.01[§]	0.27 ± 0.02^{§+}	0.21 ± 0.02⁺
<i>C</i> (ml mmHg ⁻¹)	1.21 ± 0.07	1.17 ± 0.08	1.24 ± 0.09	1.05 ± 0.06	1.36 ± 0.06	1.28 ± 0.07	1.10 ± 0.08	1.24 ± 0.08
<i>P</i> _∞ (mmHg)	11.5 ± 0.3*[‡]	14.9 ± 0.4*[†]	19.1 ± 0.4^{†‡}	14.9 ± 0.3	15.3 ± 0.3	13.5 ± 0.4^{§¶}	15.7 ± 0.4[§]	16.3 ± 0.4[¶]
Wave Analysis Results								
Wave speed (m s ⁻¹)	2.7 ± 0.1	2.5 ± 0.1	2.4 ± 0.1	2.7 ± 0.1	2.4 ± 0.1	2.6 ± 0.1	2.6 ± 0.1	2.5 ± 0.1
Absolute negative Γ (%)**	27 ± 1	29 ± 1	28 ± 2	30 ± 1	26 ± 1	28 ± 1	30 ± 1	26 ± 1
Negative reflector distance (cm)	5.0 ± 0.3	4.4 ± 0.3	4.6 ± 0.3	4.8 ± 0.2	4.5 ± 0.3	5.2 ± 0.3	4.4 ± 0.3	4.4 ± 0.3

Values represent least-squared mean values ± s.e.m. and statistical results from three-way ANOVA. Abbreviation: PEEP, positive end-expiratory pressure. Bold numbers indicate significant ($P < 0.05$) differences within each volume load, PEEP and ventilation group. Within volume load, significant ($P < 0.05$) pairwise Bonferroni comparisons are indicated: * low vs. medium, [†]medium vs. high and [‡]low vs. high. Within ventilation, significant ($P < 0.05$) pairwise Bonferroni comparisons are indicated: [§]100% O₂ vs. hypoxia; ⁺ hypoxia vs. nitric oxide; and [¶]100% O₂ vs. nitric oxide. **For these data, there is a significant interaction between volume load and ventilation [$F(4,94) = 2.818, P = 0.029$]. Therefore, the effects of volume load and ventilation cannot be interpreted singularly and Fig. 3 must be used to interpret the relation between these two factors.

as a percentage [$100 |\Gamma|$], and the estimated distance from measurement location to negative reflection site are listed in Table 1.

Table 1 shows the results of three-way ANOVA applied to the reservoir parameters, single point wave speed, negative Γ and reflector distance. The results are organized into overlapping groups to show the effects of volume loading, PEEP and ventilation condition. None of the interventions had a significant effect on the distance between the measurement location and the negative reflection site and therefore, the mean value (4.7 ± 0.2 cm) is used as an estimate for this measurement. The absolute negative Γ data cannot be properly interpreted for both volume loading and ventilation as there is significant interaction [$F(4,94) = 2.818, P = 0.029$] between these interventions. To understand these data, Fig. 3 shows the absolute negative Γ data plotted at each volume load and ventilation condition. With 100% O₂ ventilation, negative reflection strengthens with progressive volume loading.

Discussion

We used the reservoir-wave model to analyse incident and reflected wave patterns in the pulmonary arterial circulation. In the main PA, negative wave reflections were observed; these appear to have originated from the junction of the left or right PAs and lobar arteries. The location of the negative reflection site did not change but the magnitude of this negative reflection increased with volume loading during 100% O₂ ventilation.

Pulmonary artery negative reflection site

Figure 2 shows a typical example of a negative reflection in the main PA. This has also been observed in other studies

using WIA on measured PA pressure and flow/velocity (Hollander *et al.* 2001; Smolich *et al.* 2008; Dwyer *et al.* 2012); however, the reflection site is usually attributed to the bifurcation of the left and right PA. Considering that the distance from the main PA measurement site to the reflection site was 4.7 ± 0.2 cm and that it was approximately 1 cm from the pulmonary valve to the main PA measurement site, the distance from the pulmonary valve to the negative reflection site is estimated to be 5.7 ± 0.2 cm. This distance corresponds to a point no farther than the end of the lobar PAs (defined as the arteries that stem from the left and right PAs) (Gan & Yen, 1994). Detailed morphometric study of PA dimensions by Attinger (1963) indicate that these branch points have daughter/mother cross-sectional area ratios ranging

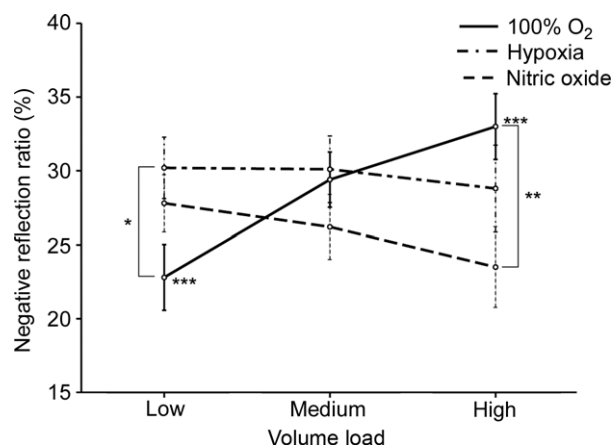


Figure 3. Negative reflection ratio as a function of volume loading for each ventilation condition

Within 100% O₂ ventilation, the absolute magnitude of negative reflection (Γ) increases. Significant Bonferroni multiple comparisons: within 100% O₂, low vs. high ***($P = 0.005$); within low volume load, 100% O₂ vs. hypoxia *($P = 0.040$); within high volume load, 100% O₂ vs. nitric oxide **($P = 0.035$).

from 0.95 to 1.22 in dogs. As shown by Attinger (1963), not all branch points are symmetrical bifurcations and therefore other studies indicate that the ratio may be as high as 1.33 in the right lung (Gan & Yen, 1994) or 1.46 from pooled data (Haworth *et al.* 1991). Negative reflections are possible if the cross-sectional area ratio of daughter/mother vessels is greater than approximately 1.2 (Parker, 2009). Therefore, as the area ratio of proximal lobar arteries to either the left or right PA may be greater than 1.2, the junction of the lobar branches offers a plausible site for negative reflection that matches the estimated distance to the reflection site from the pulmonary valve.

Strength of pulmonary artery negative reflection

The summarized results in Fig. 3 show that strength of absolute negative Γ increases approximately 10% with volume loading during 100% O₂ ventilation. This behaviour, which is consistent with the increase in conductance that accompanies volume loading (Bouwmeester *et al.* 2013), is similar to that reported by

Hollander *et al.* (2001). Volume loading apparently dilates the lobar arteries proportionally more than the left or right PAs from which they branch. Even though mechanical testing has shown no difference in the passive properties between main, left branch and lobar PAs (Cox, 1982), the response *in vivo* to volume loading remains an open question as others have reported that pulmonary vascular compliance increases from proximal to distal portions of the arteries (Altinawi *et al.* 1991; Gan & Yen, 1994).

At the low volume load, Fig. 3 shows that hypoxia has significantly stronger negative wave reflections compared to 100% O₂ ventilation. A similar study investigating the effects of hypoxia on the pulmonary circulation showed similar patterns in regards to net wave intensity (Nie *et al.* 2001). Although Fig. 2 shows that net wave intensity has the potential to mask the effects of backward waves and only indicates which wave dominates at a particular time in the cardiac cycle, the results of Nie *et al.* could be interpreted in the context of the reservoir-wave model. Their observed increases of negative net wave intensity with hypoxia would imply greater negative wave reflection, which corresponds to the increased magnitude

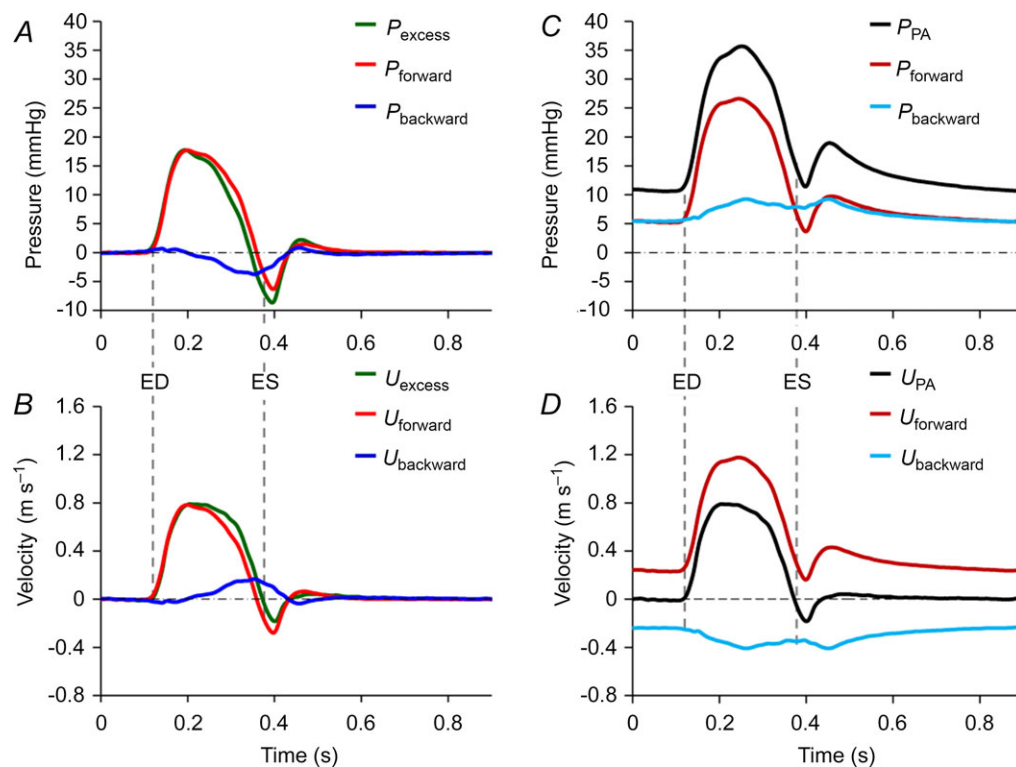


Figure 4. Pulmonary artery reservoir-wave versus conventional wave analysis

Data are taken during low blood volume, 0 cmH₂O positive end-expiratory pressure and 100% O₂ ventilation. This figure indicates the importance of subtracting reservoir pressure and velocity from the measured values before analysing wave patterns. A–D, both the pressure and velocity are decomposed into the contributions of forward-going (P_{forward} and U_{forward}) and backward-going waves (P_{backward} and U_{backward}). A, excess pressure (P_{excess}). B, excess velocity (U_{excess}). C, pulmonary venous pressure (P_{PA}). D, pulmonary venous velocity (U_{PA}). Vertical dashed lines indicate ED and ES, which were defined by the upstroke and down stroke of U_{excess} or U_{PA} crossing zero. ED, end diastole; ES, end systole.

of negative reflections at the low volume load displayed in Fig. 3. Nie *et al.* also showed less wave reflection with nitric oxide inhalation, whereas the results in our study show no significant difference in the strength of negative reflections when nitric oxide was added to hypoxic ventilation.

Reservoir-wave versus conventional wave analysis

The consequences of considering reservoir effects in the PA are illustrated in Fig. 4. The reservoir-wave model shows the importance of subtracting reservoir pressure before performing wave analysis in the main PA. Once excess pressure is determined, either the impedance approach or WIA yields identical results (Hughes & Parker, 2009). This figure shows the contributions of forward- and backward-going waves to both pressure and velocity. Results are shown of the reservoir-wave model and WIA applied separately to P_{excess} (Fig. 4A) and U_{excess} (Fig. 4B). Figure 4C and D show the conventional technique (Westerhof *et al.* 1972; Hughes & Parker, 2009) applied separately to measured P_{PA} (Fig. 4C) and U_{PA} (Fig. 4D). In Fig. 4D, equal and opposite forward- and backward-going waves balance precisely to yield zero velocity/flow during diastole. In the PA, backward-going waves are assumed reflections of forward-going waves. Therefore, zero flow during diastole can be explained simply by the closure of the pulmonary valve or alternatively, as conventional analysis implies, reflections are always present and reduce the supposed amount of forward flow provided by the RV. In Fig. 4A and B, WIA of P_{excess} and U_{excess} demonstrates a wave pattern that is entirely consistent with minimal wave activity during diastole and furthermore, a proximal negative reflection is a mechanism that augments the blood flow provided by the RV. In a sense, blood is sucked forward, which serves to decrease pressure and increase flow.

Limitations

This study was conducted in open chest, anaesthetized dogs because it was not feasible to make such extensive measurements in a more intact preparation. Thus, our conclusions should be validated using more physiological experimental models and/or clinical observations.

Reservoir parameters were calculated during diastole. When heart rate is less than approximately 80 bpm, the reservoir parameters can be determined from regular P_{PA} waveforms robustly. However, if the heart rate is greater, determining reservoir parameters for regular beats becomes more difficult. In this study, to maintain the robust ability to calculate reservoir parameters at every intervention, acetylcholine was injected to extend diastole/diastasis after a series of regular beats.

Recently, a simulation consisting of three bifurcating tubes of arbitrary length, geometry and wall properties, terminated by a three-element windkessel questioned the validity of the reservoir-wave paradigm (Mynard *et al.* 2012). This hypothetical model showed that negative reflections were amplified and positive reflections were dampened, which applied to this study, would imply that the observed negative reflections in the main PA are questionable. As discussed by Tyberg *et al.* (2014) the model used by Mynard *et al.* (2012) with elastic (i.e. no energy loss), 1-D tubes may not represent physiological pressure-volume properties and more advanced fluid-structure interaction models that take into account viscoelastic vessel properties may be required (Giannopapa, 2004; Bessems *et al.* 2008). We maintain that using real physiological measurements of pressure and flow and describing waves with excess pressure yields a plausible pattern of wave propagation and reflection during normal conditions, vasoconstriction and vasodilation (Wang *et al.* 2011, 2013) that is not possible when using impedance analysis, as demonstrated by paradoxical reflected waves that appear to propagate downstream, when they should propagate upstream (Wang *et al.* 2011; Tyberg *et al.* 2013; Westerhof & Westerhof, 2013).

Conclusions

We conclude that there are significant negative wave reflections in the main PA that arise from the junction of lobar arteries from the left or right PAs. This reflection provides a mechanism to reduce peak systolic pressure and, at the same time, increase blood flow and effectively facilitating right ventricular ejection. This mechanism is not apparent when measured pressure and flow waveforms are analysed conventionally. It is important to define this naturally occurring negative reflection to understand normal and pathological pulmonary circulatory physiology.

References

- Altinawi A, Madden JA, Dawson CA, Linehan JH, Harder DR & Rickaby DA (1991). Distensibility of small arteries of the dog lung. *J Appl Physiol* **71**, 1717–1722.
- Attinger EO (1963). Pressure transmission in pulmonary arteries related to frequency and geometry. *Circ Res* **12**, 623–641.
- Bessems D, Giannopapa CG, Rutten MCM & van de Vosse FN (2008). Experimental validation of a time-domain-based wave propagation model of blood flow in viscoelastic vessels. *J Biomech* **41**, 284–291.
- Bouwmeester JC, Belenkie I, Shrive NG & Tyberg JV (2013). Partitioning pulmonary vascular resistance using the reservoir-wave model. *J Appl Physiol* **115**, 1838–1845.

- Caro CG & McDonald DA (1961). Relation of pulsatile pressure and flow in pulmonary vascular bed. *J Physiol* **157**, 426–453.
- Castelain V, Herve P, Lecarpentier Y, Duroux P, Simonneau G & Chemla D (2001). Pulmonary artery pulse pressure and wave reflection in chronic pulmonary thromboembolism and primary pulmonary hypertension. *J Am Coll Cardiol* **37**, 1085–1092.
- Cox RH (1982). Comparison of mechanical and chemical-properties of extralobar and intralobar canine pulmonary-arteries. *Am J Physiol Heart Circ Physiol* **242**, H245–H253.
- Davies JE, Baksi J, Francis DP, Hadjiilouzou N, Whinnett ZI, Manisty CH, Aguado-Sierra J, Foale RA, Malik IS, Tyberg JV, Parker KH, Mayet J & Hughes AD (2010). The arterial reservoir pressure increases with aging and is the major determinant of the aortic augmentation index. *Am J Physiol Heart Circ Physiol* **298**, H580–H586.
- Dwyer N, Yong AC & Kilpatrick D (2012). Variable open-end wave reflection in the pulmonary arteries of anesthetized sheep. *J Physiol Sci* **62**, 21–28.
- Elzinga G, Piene H & de Jong JP (1980). Left and right ventricular pump function and consequences of having two pumps in one heart. A study on the isolated cat heart. *Circ Res* **46**, 564–574.
- Flewitt JA, Hobson TN, Wang JJ, Johnston CR, Shrive NG, Belenkie I, Parker KH & Tyberg JV (2007). Wave intensity analysis of left ventricular filling: application of windkessel theory. *Am J Physiol Heart Circ Physiol* **292**, H2817–H2823.
- Frank O (1899). Die Grundform des Arteriellen Pulses. Erste Abhandlung. Mathematische Analyse. *Z Biol* **37**, 483–526.
- Gan RZ & Yen RT (1994). Vascular impedance analysis in dog lung with detailed morphometric and elasticity data. *J Appl Physiol* **77**, 706–717.
- Giannopapa CG (2004). *Fluid Structure Interaction in Flexible Vessels*. University of London, King's College, London.
- Haworth ST, Linehan JH, Bronikowski TA & Dawson CA (1991). A hemodynamic model representation of the dog lung. *J App Physiol* **70**, 15–26.
- Hollander EH, Wang JJ, Dobson GM, Parker KH & Tyberg JV (2001). Negative wave reflections in pulmonary arteries. *Am J Physiol Heart Circ Physiol* **281**, H895–H902.
- Hughes AD & Parker KH (2009). Forward and backward waves in the arterial system: impedance or wave intensity analysis? *Med Biol Eng Comput* **47**, 207–210.
- Khiri AW, O'Brien A, Gibbs JSB & Parker KH (2001). Determination of wave speed and wave separation in the arteries. *J Biomech* **34**, 1145–1155.
- Lankhaar JW, Westerhof N, Faes TJ, Marques KM, Marcus JT, Postmus PE & Vonk-Noordegraaf A (2006). Quantification of right ventricular afterload in patients with and without pulmonary hypertension. *Am J Physiol Heart Circ Physiol* **291**, H1731–1737.
- Lankhaar JW, Westerhof N, Faes TJC, Gan CTJ, Marques KM, Boonstra A, van den Berg FG, Postmus PE & Vonk-Noordegraaf A (2008). Pulmonary vascular resistance and compliance stay inversely related during treatment of pulmonary hypertension. *Eur Heart J* **29**, 1688–1695.
- Milnor WR, Conti CR, Lewis KB & O'Rourke MF (1969). Pulmonary arterial pulse wave velocity and impedance in man. *Circ Res* **25**, 637–649.
- Mitchell JR, Doig CJ, Whitelaw WA, Tyberg JV & Belenkie I (2011). Volume loading reduces pulmonary vascular resistance in ventilated animals with acute lung injury: evaluation of RV afterload. *Am J Physiol Regul Integr Comp Physiol* **300**, R763–R770.
- Mynard JP, Penny DJ, Davidson MR & Smolich JJ (2012). The reservoir-wave paradigm introduces error into arterial wave analysis: a computer modelling and in-vivo study. *J Hypertens* **30**, 734–743.
- Nakayama Y, Nakanishi N, Sugimachi M, Takaki H, Kyotani S, Satoh T, Okano Y, Kunieda T & Sunagawa K (1997). Characteristics of pulmonary artery pressure waveform for differential diagnosis of chronic pulmonary thromboembolism and primary pulmonary hypertension. *J Am Coll Cardiol* **29**, 1311–1316.
- Nie M, Kobayashi H, Sugawara M, Tomita T, Ohara K & Yoshimura H (2001). Helium inhalation enhances vasodilator effect of inhaled nitric oxide on pulmonary vessels in hypoxic dogs. *Am J Physiol Heart Circ Physiol* **280**, H1875–1881.
- Parker KH (2009). An introduction to wave intensity analysis. *Med Biol Eng Comput* **47**, 175–188.
- Parker KH & Jones CJH (1990). Forward and backward running waves in the arteries: analysis using the method of characteristics. *J Biomech Eng* **112**, 322–326.
- Patel DJ, Defreitas FM & Fry DL (1963). Hydraulic input impedance to aorta and pulmonary artery in dogs. *J Appl Physiol* **18**, 134–140.
- Permutt S & Riley RL (1963). Hemodynamics of collapsible vessels with tone – vascular waterfall. *J Appl Physiol* **18**, 924–932.
- Sagawa K, Lie RK & Schaefer J (1990). Translation of Otto Frank's paper "Die Grundform des Arteriellen Pulses" *Zeitschrift fur Biologie* 37: 483–526 (1899).[classical article]. *J Mol Cell Cardiol* **22**, 253–277.
- Saouti N, Westerhof N, Postmus PE & Vonk-Noordegraaf A (2010). The arterial load in pulmonary hypertension. *Eur Respir Rev* **19**, 197–203.
- Scott-Douglas NW, Traboulsi M, Smith ER & Tyberg JV (1991). Experimental instrumentation and left ventricular pressure–strain relationship. *Am J Physiol Heart Circ Physiol* **261**, H1693–H1697.
- Smolich JJ, Mynard JP & Penny DJ (2008). Simultaneous pulmonary trunk and pulmonary arterial wave intensity analysis in fetal lambs: evidence for cyclical, midsystolic pulmonary vasoconstriction. *Am J Physiol Regul Integr Comp Physiol* **294**, R1554–R1562.
- Tyberg JV, Davies JE, Wang Z, Whitelaw WA, Flewitt JA, Shrive NG, Francis DP, Hughes AD, Parker KH & Wang JJ (2009). Wave intensity analysis and the development of the reservoir-wave approach. *Med Biol Eng Comput* **47**, 221–232.
- Tyberg JV, Bouwmeester JC, Shrive NG & Wang JJ (2013). CrossTalk opposing view: Forward and backward pressure waves in the arterial system do not represent reality. *J Physiol* **591**, 1171–1173; discussion 1175.

- Tyberg JV, Bouwmeester JC, Parker KH, Shrive NG & Wang JJ (2014). The case for the reservoir-wave approach. *Int J Cardiol* **172**, 299–306.
- Wang JJ, O'Brien AB, Shrive NG, Parker KH & Tyberg JV (2003). Time-domain representation of ventricular-arterial coupling as a windkessel and wave system. *Am J Physiol Heart Circ Physiol* **284**, H1358–H1368.
- Wang JJ, Flewitt JA, Shrive NG, Parker KH & Tyberg JV (2006). Systemic venous circulation. Waves propagating on a windkessel: relation of arterial and venous windkessels to systemic vascular resistance. *Am J Physiol Heart Circ Physiol* **290**, H154–H162.
- Wang JJ, Shrive NG, Parker KH & Tyberg JV (2008). Effects of vasoconstriction and vasodilatation on LV and segmental circulatory energetics. *Am J Physiol Heart Circ Physiol* **294**, H1216–H1225.
- Wang JJ, Shrive NG, Parker KH, Hughes AD & Tyberg JV (2011). Wave propagation and reflection in the canine aorta: analysis using a reservoir-wave approach. *Can J Cardiol* **27**, 389.e381–389.e310.
- Wang JJ, Bouwmeester JC, Belenkie I, Shrive NG & Tyberg JV (2013). Alterations in aortic wave reflection with vasodilatation and vasoconstriction in anaesthetized dogs. *Can J Cardiol* **29**, 243–253.
- Westerhof N & Westerhof BE (2013). CrossTalk proposal: Forward and backward pressure waves in the arterial system do represent reality. *J Physiol* **591**, 1167–1169; discussion 1177.
- Westerhof N, Elzinga G & Sipkema P (1971). An artificial arterial system for pumping hearts. *J Appl Physiol* **31**, 776–781.

- Westerhof N, Sipkema P, van den Bos GC & Elzinga G (1972). Forward and backward waves in the arterial system. *Cardiovasc Res* **6**, 648–656.

Additional Information

Competing interests

The authors have no conflicts of interest, financial or otherwise, to declare.

Author contributions

The experiments in this study were performed in the Libin Cardiovascular Institute of Alberta at the University of Calgary. J.C.B., I.B., N.G.S. and J.V.T. conceived and designed the experiments. J.C.B. collected and analysed experimental data and J.C.B., I.B., N.G.S. and J.V.T. interpreted the experimental data. J.C.B., I.B., N.G.S. and J.V.T. drafted the article and revised it critically for important intellectual content. All authors have read and approved the manuscript.

Funding

This work was supported by the Canadian Institutes of Health Research [106520].

Acknowledgements

The authors appreciate the surgical expertise of Cheryl Meek and the helpful criticisms of Dr Jiun-Jr Wang.